



Investigations of Polymethacrylate Tribochemical Films Using X-Ray Spectroscopy and Optical Profilometry

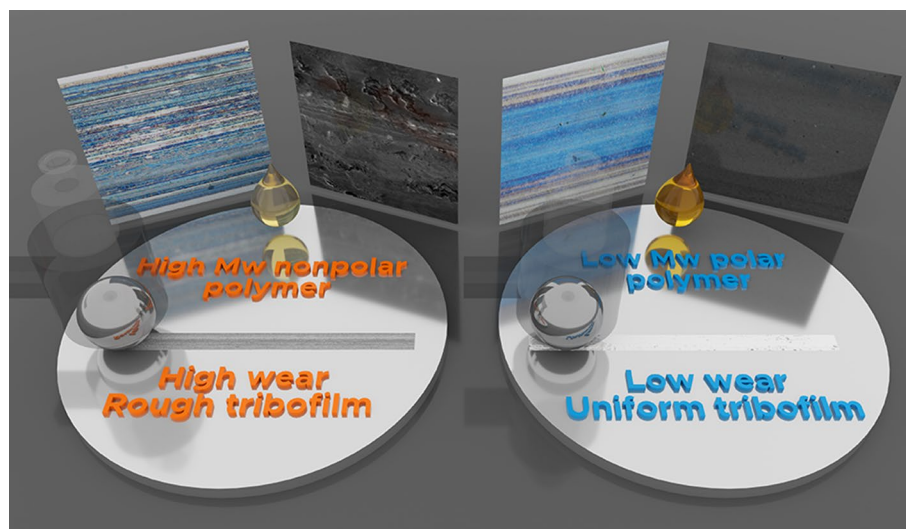
Robert A. Erck¹ · Miao Song² · Dongsheng Li² · Lelia Cosimbescu²

Received: 13 September 2020 / Accepted: 6 December 2020 / Published online: 6 February 2021
© Battelle Memorial Institute, under exclusive license to Springer Science+Business Media, LLC, part of Springer Nature 2021

Abstract

This study investigates the elemental composition and surface morphology of solid tribochemical films formed on steel surfaces. The reversible addition-fragmentation chain transfer (RAFT) method was used to synthesize nine different metal-free polymers, which were blended into commercial base oils. The polymers were either homopolymers of dodecyl methacrylate and ethylhexyl methacrylate or were co-polymers of these monomers with six polar monomers. After tribological testing at 100 °C using the ball-on-flat geometry, the resulting tribochemical films were imaged using scanning electron microscopy (SEM) and optical microscopy. The resulting tribochemical films have thicknesses around 50–100 nm. Two of the films corresponding to small (**P1**—imidazole-containing copolymer) and large (**P3**—less polar homopolymer) wear were cross-sectioned using focused ion beam (FIB) and analyzed for elemental composition using energy-dispersive X-Ray (EDX) mapping. Oxygen and nitrogen enrichment was observed, consistent with the relative chemical composition of the precursor polymers. Transmission electron microscopy (TEM) evidence suggests that at the worn surface, some organic elements penetrate or are mixed into the steel substrate giving an interlocking appearance. The two samples examined with TEM showed that **P1** tribofilm is diffused or mixed with the steel substrate more so than **P3**, suggesting a stronger affinity and contact during tribofilm formation.

Graphic Abstract



Keywords Organic tribochemical film · Polymethacrylates · Wear · Transmission electron microscopy · Scanning electron microscopy · Optical imaging

Extended author information available on the last page of the article

1 Introduction

Lubricants are used in vehicle engines and in machinery to reduce friction and wear, dissipate heat, prevent corrosion and oxidation, and often remove or sequester [1]. The efficiency of engines may be increased by lowering oil viscosity, thereby minimizing hydrodynamic shear losses. On the other hand, with lower viscosity comes greater asperity contact, which leads to lubrication moving from hydrodynamic (thick film), to mixed, or to boundary (thin film) regime. With the advent of less viscous fluids, viscosity modifiers, friction modifiers, and antiwear additives become more important in compensating for the reduced surface separation by such oils and increase service life. There are four classes of friction modifier additives: (1) organic friction modifiers which include amine and free fatty acids; (2) organo-molybdenum compounds; (3) functionalized polymers which adsorb on polar surfaces and reduce friction in some contact conditions; and (4) nanoparticles. Several reviews present advancements and challenges with each class [2–4].

Organometallic additives such as zinc dialkyldithiophosphates (ZDDP) [5], molybdenum dithiocarbamate (MoDTC), and molybdenum dithiophosphate (MoDTP) [6, 7] are widely used effective antiwear and friction modifiers via reaction with metal surfaces to form protective coatings and suppressing surface wear, but may produce unacceptable SAPS (sulphated ash, phosphorus, and sulfur) emissions [8, 9]. Although not currently adopted by industry, additives which are free of these hazardous components are desirable; a need for them can become critical especially if driven by environmental considerations. In this context, multifunctional ashless additives may be useful for performing several functions (viscosity index, antiwear, friction reduction) while decreasing the complexity of lubricant formulations. There are many reports of functionalized polymers that offer friction reduction along with competitive viscosity index improvements [3, 10–15].

Our research efforts have shown that modestly polar polymers can contribute efficiently to surface protection, presumably due to a formed polymer layer that prevents hard contact between the two shearing solid surfaces. In addition to surface protection, the adsorbed polymers may also aid in friction reduction or stabilization. By definition, a friction modifier reduces friction or stabilizes the coefficient of friction (COF) profile. In our experience, polymers that have large enough molecular weights (M_w) to be efficient viscosity index improvers (VIIs) only offer marginal friction and wear benefits, if any [16, 17]. If the primary function of the polymers is as VIIs, then by design, they have high molecular weights, which in turn results in permanent shear thinning due to mechanical cleavage of chemical bonds during shear [18–21]. To mitigate the shear losses, lower

M_w polymers can be employed as VIIs. We reported in the past multifunctional polymers that offered competitive VIIs, superior shear stability versus commercial benchmarks, and wear protection [22]. These low molecular weight analogs (homopolymer and co-polymers) had a low and broad M_w (40–60 kDa with polydispersity 5–7,) as they were prepared via free radical polymerization and required up to 12% w/w/ polymer in a Group III base oil whose viscosity at 100 °C is 4 cSt, to obtain competitive viscosity indexes (VIs). Although these compounds provided good shear stabilities, and high VIs, they provided only a modest wear benefit, albeit their large concentration required. Recently, we reported similar linear polymers with higher but narrow molecular weights (M_w 130–170 kDa, with polydispersity 1.5–2), prepared via Reversible Addition-Fragmentation Chain Transfer (RAFT), which were designed specifically for shear stability, VI performance, and antiwear [23]. The polar moieties included the following: vinylimidazole (VIIm), hydroxyethylmethacrylate (HEMA), methacrylic acid (MA), glycidylmethacrylate (GlyMA), and 2-(dimethylamino)ethyl methacrylate (DMAEMA). We also introduced polarity via boronate ester in the molecular design using free radical polymerization with a vinyl monomer (RAFT was inefficient toward copolymerization with DMA). The rheology of these polymers, wear, friction, and shear stability were evaluated in a 70%100R/30%220R (w/w) base oil at only 2% (w/w) and compared to a commercial benchmark utilized in hydraulic fluids for fluid power applications. Molecular weights ranged from 120 to 170 kDa, and the resulting VIs in general correlated with M_w . The COF of all compounds were comparable to the commercial benchmark, except the lowest molecular weight polymer which showed a significant friction reduction (25%). The low molecular weight imidazole-containing polymer produced much less wear (<4%) than did the commercial standard followed by the higher molecular weight polymers containing imidazole, hydroxy group, and amino group, respectively. This result supports our hypothesis that polar moieties have a higher affinity for the surface and provide wear protection. Molecular weight correlated well with shear stability (via KRL at 100 °C) suggesting that it is the main driver in shear stability losses alongside architecture, and several polymers displayed very low viscosity losses, comparable to those of the commercial benchmark between 2 and 5%. However, until now, we have not attempted to analyze the flat surfaces of the wear tracks. Although X-ray spectroscopy has been widely employed to analyze tribochemical films induced from ionic liquid friction or ionic liquid in combination with zinc dialkyldithiophosphate, similar studies from non-metallic organic compounds that do not contain phosphorus or sulfur are not known in the published literature [24–29]. In this work, via SEM and TEM analysis of the flat surfaces after friction (ball-on-flat) for 1 h, at 100 °C, we probe for

the presence of chemical tribochemical films, understand the nature of the interfaces, and investigate whether they correlate to wear performance. This analysis will enable a better assessment of the structure–wear relationship, as well as prove the utility of polymers as antiwear additives, and help future molecular designs of advanced materials.

2 Experimental

The synthesis and characterization of the polymers and their oil solution bulk rheology properties (kinematic viscosities, viscosity indexes, and shear) are not discussed here as they are reported elsewhere [23]. Wear is presented here in some detail, as it is pertinent to the flat-surface analysis evaluation and serves as a cross check for tribochemical film formation.

2.1 Lubricant Test Samples

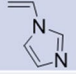
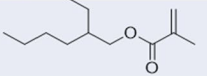
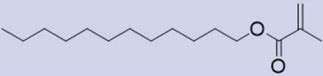
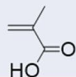
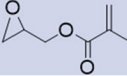
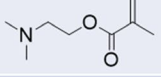
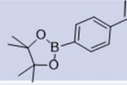
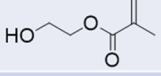
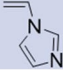
Polymers with controlled molecular weights containing nitrogen, oxygen and boron as potential polar surface anchors, were prepared, with the expectation that they would display reduced wear based on their surface affinity. The list of co-monomers utilized in the synthesis and their feed ratios, as well as their M_w , are reported in Fig. 1.

Polymers were dissolved in a mixture of two base oils commonly used in hydraulic fluid formulations, 70%100R/30%220R (w/w), at a concentration of 2% w/w. The base oils were combined as such, to achieve a specific viscosity near 4 cSt at 100 °C. The polymer solutions in base oil had the following KV100: 6.00 cSt (**P1**), 6.380 cSt (**P2**), 6.440 cSt (**P3**), 5.52 cSt (**P4**), 6.90 cSt (**P5**), 7.10 cSt (**P6**), 6.95 cSt (**P7**), 5.75 cSt (**P8**), and 6.63 cSt (**P9**). These polymer solutions were utilized for subsequent friction and wear measurements as described below.

2.2 Tribology Procedure

A modified TE 67/R Plint tribometer, with the plate driven by a motor through a Scotch Yoke mechanism, was used to produce reciprocating motion. Instantaneous friction force measurements were obtained by a piezoelectric load cell (Kistler 9332A) and amplifier (Kistler 5010). A ball-on-flat geometry was employed in which the stationary upper specimen was a hardened-type 52100 steel (HRC62, $S_a = 15$ nm) ball $\frac{1}{2}$ " diameter, and the flat reciprocating lower specimen, the "plate," had roughness $S_a = 6$ nm, obtained by lapping type 52100 steel coupons (HRC62). The test temperature was 100 °C and the test duration was 1 h. The stroke length was 20 mm and the reciprocation rate was 2 Hz. A deadweight load of 15.6 N was used to produce a peak initial static

Fig. 1 Polymer composition, molecular weight, monomer feed, and structure. **P2** and **P3** are homopolymers of the monomers indicated in the respective column, while all other polymers are co-polymers of DMA and a monomer indicated in the "polar monomer" column

Polymer	Polymer Composition	Polar Monomer	\bar{M}_w^{app} (kg/mol)
P1	Poly(DMA-co-V-imidazole) (250:50)		45.6
P2	Poly(EHMA) (750)		151
P3	Poly(DMA) (750)		126
P4	Poly(DMA-co-MA) 675:75		137
P5	Poly(DMA-co-glycidyl) 625:125		171
P6	Poly(DMA-co-DMAEMA) 625:125		156
P7	Poly(DMA-co-boronate)		150
P8	Poly(DMA-co-HEMA) 625:125		124
P9	Poly(DMA-co-V-imidazole) 625:125		59.6

Hertzian pressure of 1 GPa, with an initial circular Hertzian contact patch of 180 μm diameter. The added fluid quantity was about 120 mm^3 which, due to surface tension, produced a small pool of oil surrounding the ball/plate contact area. The sliding was in the boundary regime where λ , or specific film thickness, was always much less than unity. The largest film separation is obtained for Hertzian contact at the start of test **P6** (highest viscosity) with highly polished specimens at mid-stroke. For a sphere-on-plane contact geometry with parameters of 7.1 cSt fluid viscosity, entrainment speed of 0.063 m/s, pressure viscosity coefficient of 9 GPa^{-1} , density of 0.78 g/ml at 100 °C, modulus of elasticity of 210 GPa, Poisson's ratio of 0.3, load of 15.6 N, the minimum film thickness is 9.82 nm, the λ ratio is 0.422 for ball and flat roughness of 6 nm and 15 nm. After sliding occurred, roughening and rough tribochemical film production reduced the λ ratio further.

2.3 Optical Imaging

After cleaning with isopropyl alcohol and wipes to remove oil, post-test optical images of the ball and plate were obtained using an Olympus STM6 metallurgical microscope. This washing removes debris, oil, degradation products, or non-adsorbed polymers from the surface. Track images were obtained very close to mid-stroke. In no instances were differences in appearance observed along the length of the track on the plate.

Post-test profilometric images of the balls and quantitative wear data were obtained using a Bruker GTK white-light interferometer (WLI) using Vision software. Wear of the ball was calculated after mathematically removing the curvature using Bruker Vision software. Two tests were performed for each polymer solution, and both values as well as the average are reported in Fig. 2. The imaging procedure

was similar for the plate, and examples from **P1** and **P3** are shown in Figs. 4, 5, and 6.

2.4 Scanning Electron Microscopy (SEM)

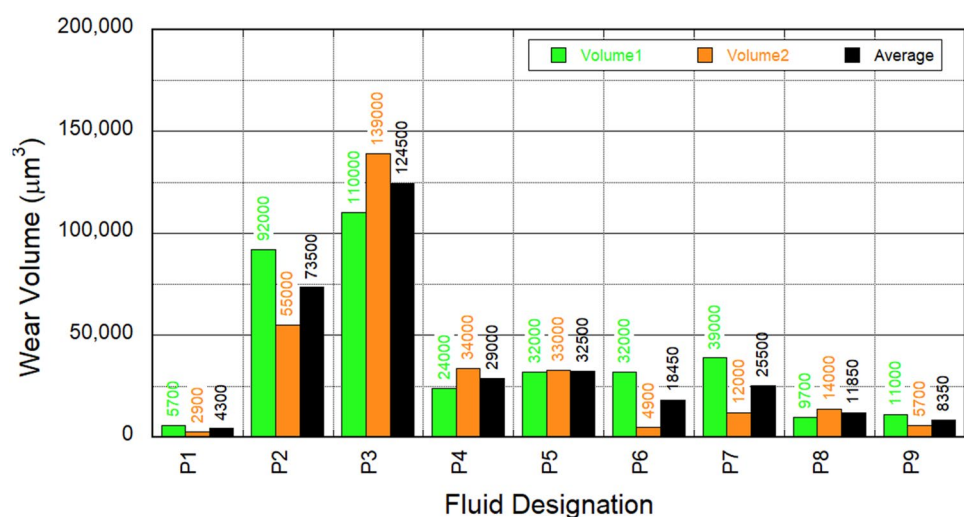
The metal plate was washed with hexanes, dichloromethane, and acetone to remove oils and residues that accumulated during friction measurements, prior to SEM measurements. The washing procedure potentially removed loose polymer or degradation products, not adsorbed or fused to the metal plate. A scanning electron microscopy (SEM, Helios NanoLab 600i, Thermo Fisher Scientific) equipped with an energy-dispersive x-ray spectrometry (EDS, Oxford Instruments, Oxfordshire, UK) was employed at 0.17 nA/5 keV for imaging and low-magnification composition analysis. In order to qualitatively compare the composition of light elements (such as O and N), which is challenging for EDS, we conducted the elemental analysis at the same conditions for all samples, including voltage (5 keV), current (0.17nA), tilt angle (15°), and collection time (~5 min).

2.5 Transmission Electron Microscopy (TEM)

2.5.1 TEM Sample Preparation

The TEM sample of cross-section lamella was prepared using a combination scanning electron and focused ion beam microscope (Helios Nanolab DualBeam, 600i ThermoFisher) as follows. To reduce the ion beam damage during TEM samples preparation process, a 5 nm Pt protection layer was deposited on the top of the film at room temperature using a sputter coater (208HR, Cressington, UK) equipped with a high-resolution thickness monitor. A sputter current of 60 mA was employed. Another ~1 μm platinum protection layer was deposited on the sample using focused ion beam in SEM. TEM lamella were then cut by a

Fig. 2 Wear volumes of the ball (two trials and their average) for each copolymer and homopolymers



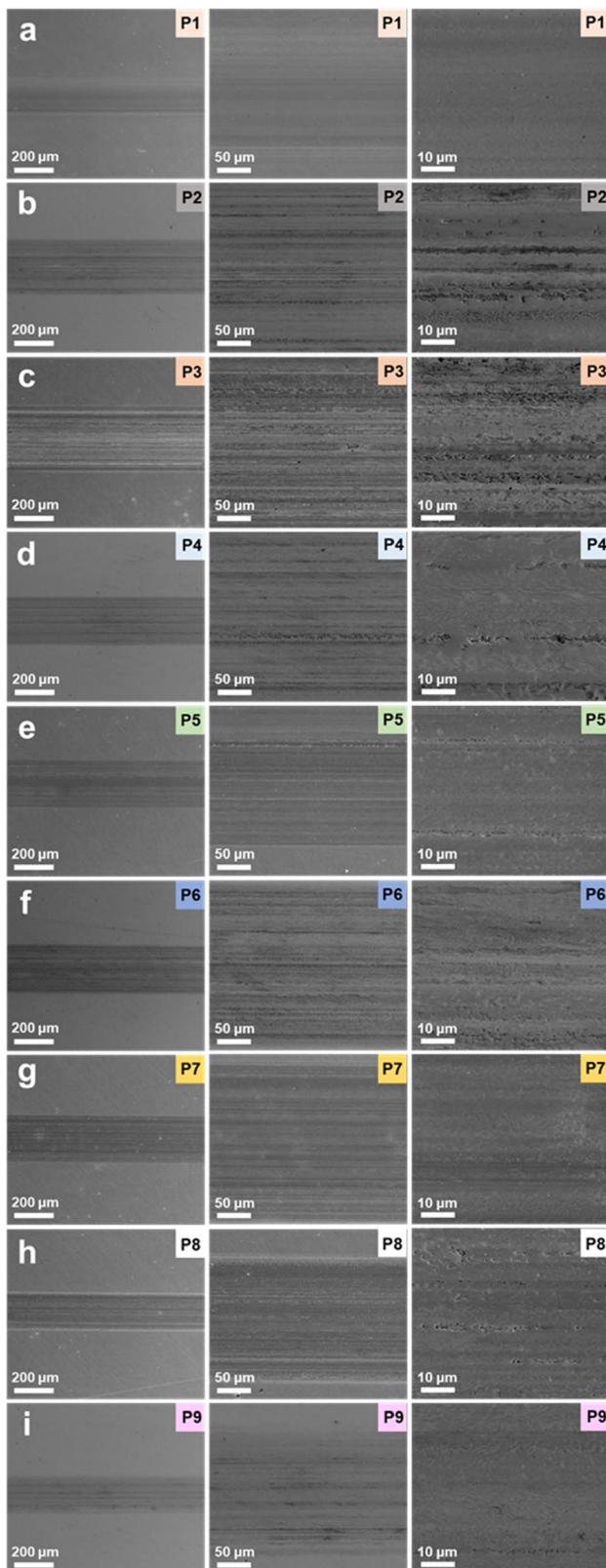


Fig. 3 SEM images of polymers **P1–P9** at differing magnifications

gallium-based focused ion beam (FIB, Helios NanoLab 600i, Thermo Fisher Scientific). During this process, the TEM samples were first milled at 0.28 nA/30 keV and then fine-milled by ion beam using low energies (28 pA/5 keV and 28 pA/2 keV) to minimize ion damage on samples.

2.5.2 TEM Characterization

An aberration-corrected TEM (Titan from Fisher Thermal, USA) equipped with a high-angle annular dark-field (HAADF) detector and an EDS system was employed at 300 kV for HAADF scanning TEM and elemental composition analysis. TEM elemental analysis was conducted at the same conditions. Films **P1** and **P3** (Fig. 1), with the best and worst performance, were selected for TEM characterization.

2.5.3 Thickness Measurement

The detailed thickness measurement of tribochemical films is as follows: (1) outline interfaces of the sample/Pt protection layer and the sample/steel substrate (relative clear interface was chosen, not including the penetration regions, as shown in Fig. S23 in the Supplemental Information) and (2) the thickness between two identified interfaces at ~ 200 nm equal intervals.

3 Results and Discussion

3.1 Effect of Polar Co-monomers on Wear

After the friction experiments were run, the balls were profilometrically examined to quantify wear. The ball wear volumes of all analogs are shown in Fig. 2. The amount of wear is increasing in the order **P1** (imidazole), **P9** (imidazole), **P8** (hydroxy), **P6** (amine), **P7** (boronate ester), **P4** (carboxylic acid), **P5** (glycidyl), **P2** (ethylhexyl), **P3** (dodecyl), and generally decreases with the polarity of the pendant in the comonomer. All polar co-polymers had wear volumes ranging from 4.3 to $32.5 \times 10^3 \mu\text{m}^3$, which were far lower compared to the non-polar homopolymers that ranged from 73.5 to $124 \times 10^3 \mu\text{m}^3$.

P2 comprised of a shorter chain C6-ethyl (EHMA) compared to **P3** (C12, DMA) is slightly less hydrophobic, which could explain the lower wear volume of **P2** versus **P3**. The most polar compounds, **P1**, **P9**, and **P8**, containing imidazole and hydroxy pendants, respectively, have the lowest wear volume.

Previous research utilized commercial benchmarks which can serve as comparative examples for this work [30]. For a 5W30 ILSAC GF5 fully formulated synthetic passenger car motor oil (11 cSt 100 °C), ball wear volume was $16,200 \mu\text{m}^3$. For a synthetic polyalphaolefin basestock oil (4.1 cSt,

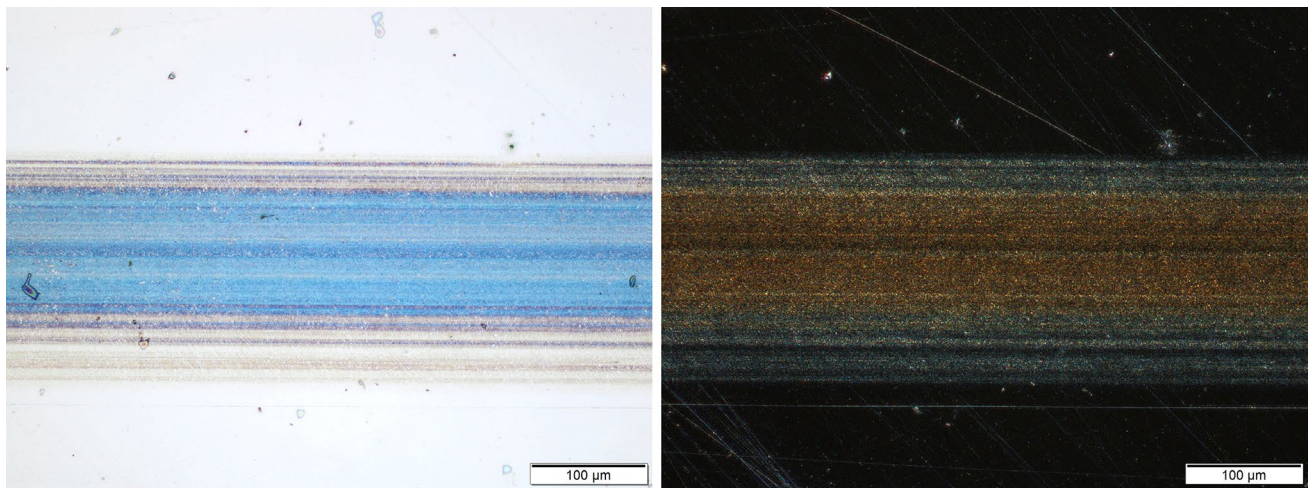


Fig. 4 Image of wear track of **P1** using conventional reflected illumination (left) and oblique illumination (right) (Color figure online)

100 °C), ball wear volume was 193,000 μm^3 . Finally, for an ISO-L-EGD JASO FD ester oil (7.88 cSt 100 °C), ball wear volume was 42,000 μm^3 . As expected, the base oil displayed the highest wear; however, the 5W30 oil shows comparable wear to several of the polymer solutions (**P1**, **P9**, **P8**), while the other fully formulated oil displays wear comparable to that of all polymer solutions, but **P2** and **P3**.

It is important to note that these co-polymers have random topologies; block co-polymers with the same polarity content would have more efficient surface interaction and would be expected to have even lower wear. Consistent with previous studies [17, 18] already referenced in the introduction, the results illustrate that polar co-polymers provided substantial wear reduction.

3.2 Scanning Electron Microscopy of Wear Flats

Encouraged by the superior wear-reducing properties of some of the polymers, based on the wear of the ball, the wear scars generated on the flat surfaces were imaged via SEM. Figure 3 shows the SEM micrographs for wear scars generated by all nine polymers. It is quite visible that the measured wear correlates well with the base scar size generated by the polymer-containing oils, and in the case of the top performing compounds, they are narrower and shallower (**P1** and **P9**) than that of the others. Grooving is sparse with interspersed darker lines that appear relatively smooth and their deformation grooves are not even visible on magnification, especially for **P1** (Fig. 3a). In contrast, the less polar polymers **P2** and **P3** produced a wear scar with many tightly spaced longitudinal grooves, whose higher magnification micrographs (Fig. 3b and c) show indication of abrasive and adhesive wear.

The results from SEM images of **P2**, **P3**, and **P4** are consistent with the higher wear data shown in Fig. 2, displaying

higher abrasions and grooving. **P1** and **P9**, the imidazole-containing compounds, and **P7**, the boronate aromatic containing polymer, which displayed lowest wear, also have the smoothest surfaces, without visible rubbing channels. **P6** (amine analog) appears to have more surface defects; however, on average, it has a relatively low wear as well. The wear values of **P6** and **P7** display a wider range of values, and coupled with the SEM data, it suggests that these compounds have variable performance and can lead to various morphology surfaces. The SEM result of **P8**, the hydroxy containing analog, does not seem to correlate well with the wear data, as it is showing a relatively rough surface, but it displays one of the lowest wear values.

3.3 Optical Imaging Studies

Our in-depth analysis of the tribochemical films of flats will focus on the most non-polar analog which displays the highest wear (**P3**), and the vinylimidazole analog (**P1**), which displays the lowest wear from ball evaluation. Secondary electron contrast is useful for imaging the physical surface, but additional imaging can be performed to understand tribochemical film morphology. Figure 4 shows optical images of wear tracks of **P1**. On the left, the wear track appears blue due to optical interference within the semi-transparent tribochemical film. The image on the right was obtained using off-normal conventional illumination to highlight a relatively thick tribochemical film indicative by the brownish color. The imaged areas are identical.

Figure 5 shows optical images of wear tracks of **P3**. In contrast to **P1**, the film is very irregular, and it is possible to clearly distinguish the patchiness and unevenness of the tribochemical film. The middle of the film shows patches that are free of tribofilm, suggesting removal of the film during friction or post-evaluation cleaning. Regardless of

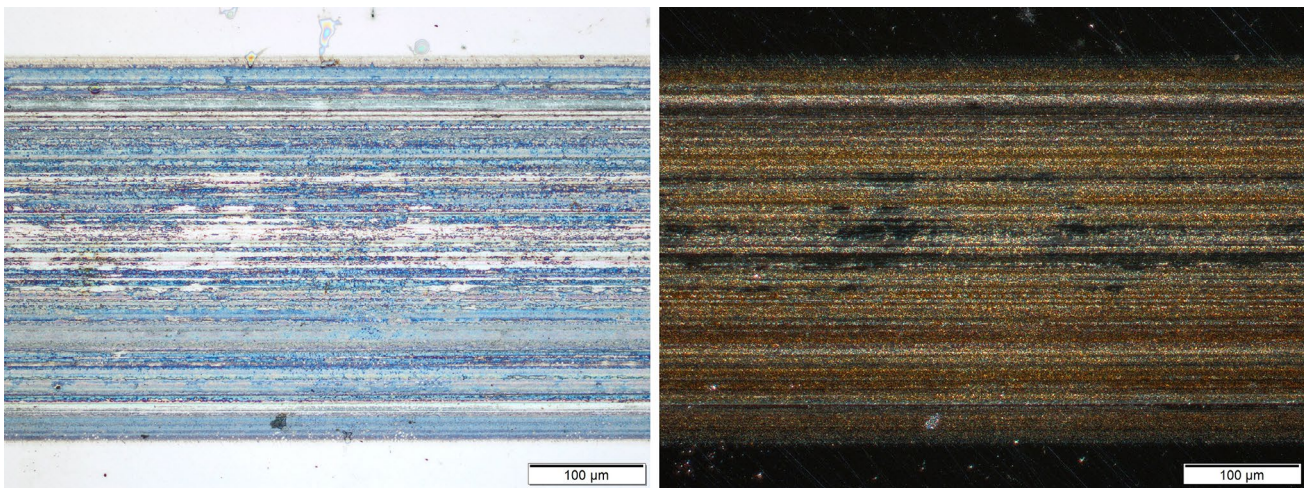


Fig. 5 Image of wear track of **P3** using conventional reflected illumination (left) and oblique illumination (right) (Color figure online)

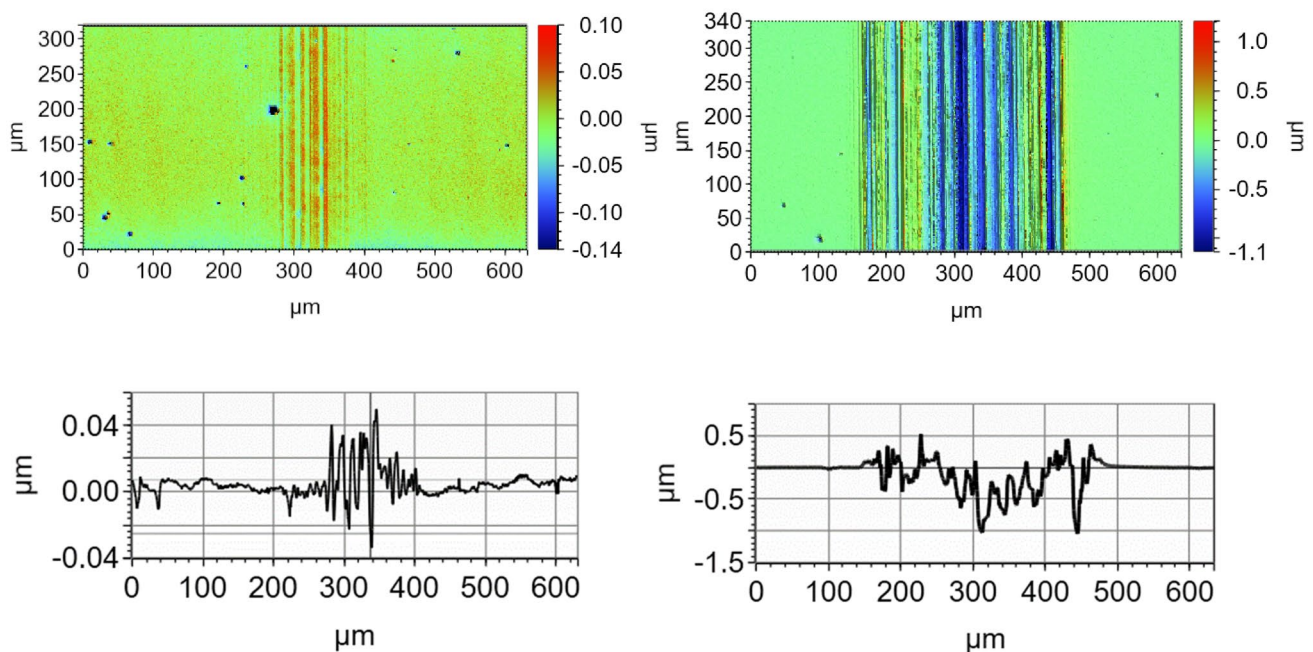


Fig. 6 Upper left: **P1** false color topography of surface, lower left: corresponding topography scan across image; upper right: **P3** false color topography of surface; lower right: corresponding topography scan across image

the cause of film removal, this observation further confirms that the least polar analog **P3** is not as tightly bound to the metal surface as **P1**.

To gather vertical information, white-light interferometry was used to image the topography of the **P1** and **P3** wear tracks. The images are shown in Fig. 6. For these studies, a thin light-reflective layer sufficient for complete reflection (about 300 nm) was deposited onto the sample using sputter coating in Ar to provide true topography of the surface and eliminate refraction effects as the analysis light penetrates the semi-transparent tribofilm and is reflected by the

substrate metal. This layer is conformal and has no effect on the tribochemical film. For **P1**, the tribochemical film is shown to be built up on the surface to typical thicknesses of (50–100) nm. In contrast, the wear scar of **P3** shows the substantial wear and grooving of the flat. In this case, it is clear that during the hour-long test, the formation of the tribochemical film was insufficient to prevent wear occurring during the test, and a dynamic system of material removal/film deposit occurred. In the microscope image above, Fig. 5, we suspect that the film-denuded areas near the center of the track were subsequently abraded after initial formation of the

Table 1 Estimated roughness and volumes for sliding tracks on the flat

Polymer tribofilm	Sa roughness (nm) of wear track	Measured average track volume μm^3 per μm of track length
P1	18	+0.54
P2	69	+13
P3	269	-55
P4	50	+11
P5	36	+10
P6	22	+6.5
P7	25	+12
P8	43	+7.4
P9	63	+7.1
Substrate	5.2	-

tribofilm, then re-coated with newly formed tribochemical film. All gold-coated and uncoated optical images of flats are shown in the Supplemental Information.

The roughness of all films was measured by examining the wear track areas on the gold-coated side and reported in Table 1. The amount of ball wear, shown in Fig. 2, is indicative of the effectiveness of the fluid formulation at preventing wear of a counterface (the ball) which is sliding on the flat. The roughness of the tribochemical film, shown in Table 1, is a geometrical property of that film which is deposited on the flat. It is not necessary that there be a relationship between the two: a smooth film may be abrasive to the counterface, and vice versa. However, for the tests performed here, there is a rough association between wear and roughness. Clearly, analogs **P1** and **P3**, with the smallest and largest wear also display the smallest and largest roughness, respectively.

It is difficult to report a flat wear volume that is meaningful due to roughening and presence of a tribochemical film. Using the tools available, it is not possible to separate wear, which is a removal process, with tribochemical film production, which is an additive process. For thick dielectric films where the primary and secondary interference fringes are well separated, it is possible to calculate film thickness if the index of refraction is known. In this case, the tribochemical film thickness is small compared to the wavelength of light. However, for the sake of completeness, Table 1 contains track volume measurements obtained from the WLI data. The track volume is defined as that amount of material removed or added per μm of track length. For example, the **P3** wear track is the most severe and a wear volume is measured as $55 \mu\text{m}^3$ per μm of sliding length. However, for **P2** the wear scar is raised above the surface, with a growth volume of $+13 \mu\text{m}^3$ per μm of sliding length.

Because the wear track width is about $180 \mu\text{m}$, the average height is about 36 nm. The Supplemental Information shows white-light images of the flat.

3.4 Transmission Electron Microscopy Characterization of the Wear Flats

To identify the microstructure and compositional differences between the two extreme analogs that show the lowest and highest wear, respectively, **P1** and **P3**, the cross-section lamella of thin films denoted **P1** and **P3** were prepared and investigated via TEM. The thicknesses of the **P1** and **P3** films are ~ 30 and ~ 80 nm, respectively (Fig. 7 and Table 2). Results of energy-dispersive X-ray spectroscopy show nitrogen and oxygen enrichment in film **P1** (denoted by yellow dashed lines in Fig. 7), consistent with the chemical composition of the polymer **P1** (Fig. 1). Film **P3** shows the presence of oxygen, but absence of nitrogen (Fig. 7d and Table 2), consistent with the composition of the polymer **P3**.

Notably, in some areas, the organic elements penetrate into the steel substrate forming nano-pillows projections (white arrows in Fig. 7b) and we hypothesize that this happens during the wear test and subsequent deposition of the tribochemical film onto the substrate due to the roughness of the steel substrate. As presented in Fig. 7e and f, the density of the penetration areas in **P1** is significantly higher, while the size is smaller than that of the sample **P3**.

In Fig. 7e and f, there are what look like vortices in the tribochemical film/steel interface. These are consistent with MD calculations of sliding interfaces as reported in other work [31].

The two EDS spectra of the extreme analogs **P1** and **P3** are shown in Fig. 8b and e. The small circles in the TEM images (8a and d) denote the area analyzed and the corresponding EDS spectra. Although the N peak intensity is low, it is ample evidence of N presence in the **P1** tribofilm versus **P3**. Its low abundance is expected, as the theoretical amount of N in the original polymer based on a 250:50 equivalents ratio of the two monomers is 2% (w/w). In fact, these studies suggest higher nitrogen content of the tribofilm, which supports the common belief that polar moieties have higher affinities for surfaces, and in this case, the surface may have been enriched in imidazole.

Based on the specific microstructure of the sample/substrate interfaces, it appears there is diffusion (penetration areas) in the sample **P1**, indicative of a strong contact between the steel substrate and tribochemical film (see the difference between Fig. 7e and f). The average interfacial structures of the two analogs illustrated in Fig. 8c and f emphasize the effect of **P1** close contact/interaction with steel surface, compared to **P3**.

Whether this kind of diffusion is induced by heating or rubbing during the wear test, one can envision that all

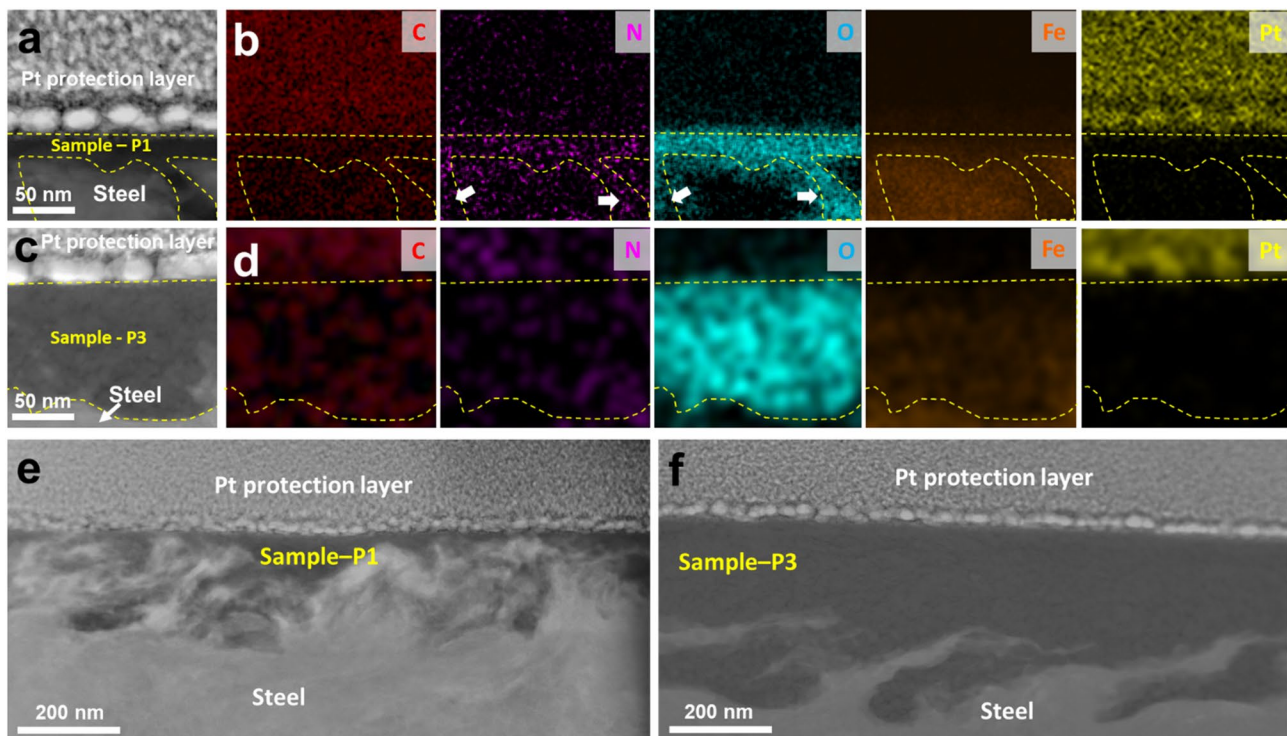


Fig. 7 Composition analysis of **P1** and **P3** films. **(a)** and **(c)** High-angle annular dark-field (HAADF) images of TEM cross-section lamella samples of **P1** and **P3**, respectively. The polymer film regions were roughly outlined by yellow dashed lines. **(b)** and **(d)** EDS map-

ping of the areas of **(a)** and **(c)**, respectively. **(e)** and **(f)** HAADF images of **P1** and **P3** showing typical microstructures of the sample/steel substrate interfaces (Color figure online)

Table 2 Sample thickness and rough quantitative composition analysis based on HAADF-EDS

Sample	Thickness ^a (nm)	Composition ^b		
		O %	C %	N %
P1	30.3 ± 12.4	54.4 ± 8.8	40.5 ± 5.5	5.1 ± 4.6
P3	81.0 ± 42.0	51.2 ± 5.5	47.7 ± 5.3	1.1 ± 0.5

^aThicknesses are estimated from the average of ~20 locations at ~200 nm equal interval (see methods for detailed thickness measurement)

^bCompositions are derived from the average value of three areas

polymer adhering to the surface may diffuse into the steel substrate changing it with time, which would make the **P1** polymer not only a shear stable viscosity modifier, but a competitive antiwear and friction modifier.

4 Conclusions

This study of tribochemical films formed from organic, non-metal containing polymers, is the first of its kind. Previous work showed that the low molecular weight imidazole-containing polymer **P1** produced much less wear (<4%)

than the non-polar counterparts, **P2** and **P3**, followed by the higher molecular weight polymers containing imidazole (**P9**), hydroxy group (**P8**), and amino group (**P6**), respectively (see Fig. 1 for structures, and Fig. 2 for wear volumes). In this work, we analyzed the flat wear scars to identify and characterize tribochemical films as well as confirm the trend observed in the ball wear.

The SEM results are generally consistent with the wear values derived from the ball missing volume, and particularly confirming the rough, irregular surfaces of the worst (non-polar polymers **P2** and **P3**) and the smooth, even surfaces of the best candidates (**P1**, **P9**, **P7**). **P8**, the hydroxy containing candidate, however, was an exception, in that the wear value was low, yet the surface appeared rugged. Optical and profilometric images further corroborated the SEM imaging, as well as confirm the presence of chemical tribofilms with varying rubbing effects. Substantial differences were noted in the extreme analogs, **P1** versus **P2** and **P3**, while the rest displayed subtle differences via optical imaging. While it is impossible to accurately determine what fraction of the profile is wear and what fraction is adhered tribofilm, profilometry examination allows for an estimation of roughness (Table 1). For the tests performed here, there is a broad association between wear and roughness. Clearly, analogs **P1** and **P3**, with the smallest and largest wear, also

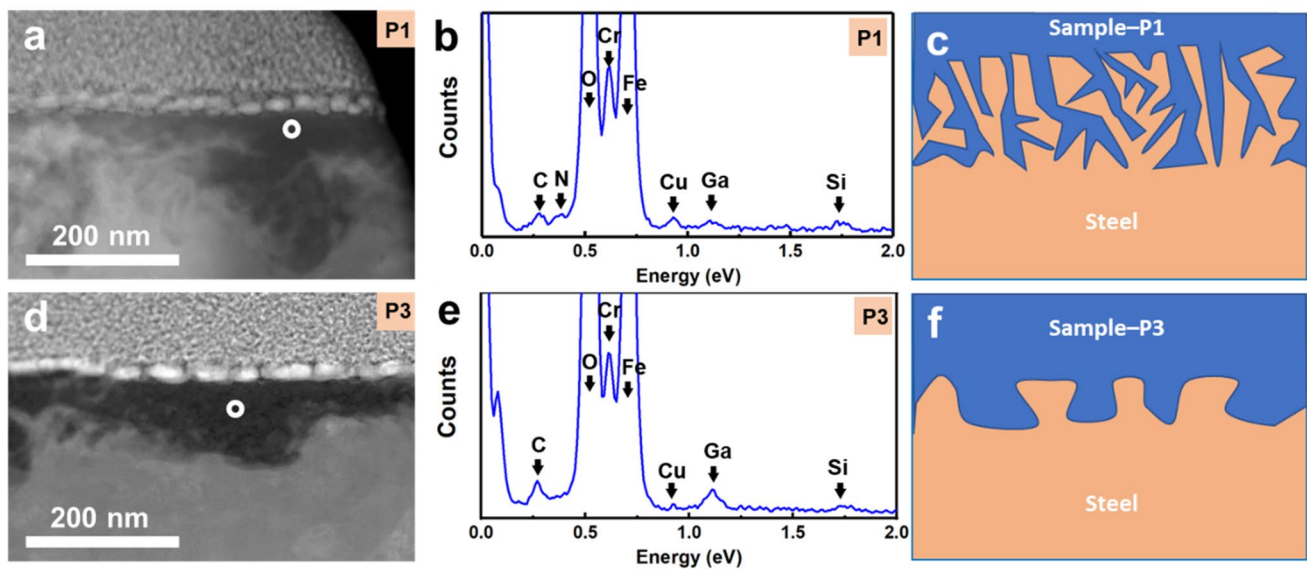


Fig. 8 Representative EDS spectra of **P1** and **P3** (middle) for the regions denoted in the TEM (left) and depiction of potential interfacial structures of steel and tribochemical films (right)

display the smallest and largest roughness, respectively. Microstructure and compositional differences were only studied via TEM for the two extreme analogs, **P1** and **P3**. The thicknesses of the **P1** and **P3** films are ~ 30 and ~ 80 nm, respectively (Fig. 7 and Table 2) and their composition evaluated by EDX is consistent with the composition of the parent polymers, with **P1** containing nitrogen, while **P3** does not. Interestingly, **P1** tribofilm appeared to have intermixed with the steel substrate more so than **P3**, suggesting a stronger contact or bond during tribofilm formation, which is thought to be one of the main reasons for its excellent anti-wear properties. Overall, these studies corroborate previous wear findings and support the conclusion that certain polar polymethacrylates have high affinities for the surface and form uniform beneficial tribofilms.

Supplementary Information The online version contains supplementary material available at <https://doi.org/10.1007/s11249-020-01388-5>.

Acknowledgements This project was funded by the Office of Vehicle Technology (VTO) of the U.S. Department of Energy (US DOE), (under Contract VT0604000-05450-1004897). PNNL is proudly operated by Battelle for the U.S. DOE (under Contract DE-AC06-76RLO 1830). The authors kindly acknowledge contributions from our colleague Mr. Cortland Johnson (PNNL) for improving the TOC graphic.

Author Contributions LC proposed the study, analyzed results, and coordinated collaborations. RE conducted friction experiments, analyzes ball and flat surfaces for wear, acquired and analyzed optical images, and interpreted all data. MS and DL acquired SEM and TEM and interpreted data. All authors wrote and reviewed this manuscript.

Data Availability Optical and profilometry images (gold-coated and uncoated) and EDS mapping of all tribochemical films are available to download from the Supporting Information, free of charge.

Compliance with Ethical Standards

Conflict of interest The authors declare no competing financial interest.

References

- Bardasz, E.A.: Lubricant Additives and Their Functions. ASM Handbook. Friction, Lubrication, and Wear Technology, vol. 18, pp. 135–149. ASM International (2017)
- Tang, Z., Li, S.: A review of recent developments of friction modifiers for liquid lubricants (2007–present). *Curr. Opin. Solid State Mater. Sci.* **18**, 119–139 (2014)
- Spikes, H.: Friction modifier additives. *Tribol. Lett.* **60**, 5 (2015)
- Guegan, J., Southby, M., Spikes, H.: Friction modifier additives, synergies and antagonisms. *Tribol. Lett.* **67**, 83 (2019)
- Spikes, H.: The history and mechanisms of ZDDP. *Tribol. Lett.* **17**, 469–489 (2004)
- Erdemir, A.: Review of engineered tribological interfaces for improved boundary lubrication. *Tribol. Int.* **38**, 249–256 (2005)
- Korecek, S., Jensen, R.K., Johnson, M.D., Sorab, J.: Fuel efficient engine oils, additive interactions, boundary friction, and wear. *Tribol. Ser.* **36**, 13–24 (1999)
- Ueda, F., Sugiyama, S., Arimura, K., Hamaguchi, S., Akiyama, K.: Engine oil additive effects on deactivation of monolithic three-way catalysts and oxygen sensors. *SAE Trans.* 332–341 (1994). <https://doi.org/10.4271/940746>
- Bodek, K.M., Wong, V.V.: The effects of sulfated ash, phosphorus and sulfur on diesel aftertreatment systems—a review. *SAE Technical Paper*; (2007). <https://doi.org/10.4271/2007-01-1922>

10. Wright, R.A., Wang, K., Qu, J., Zhao, B.: Oil-soluble polymer brush grafted nanoparticles as effective lubricant additives for friction and wear reduction. *Angew. Chem.* **128**, 8798–8802 (2016)
11. van Ravensteijn, B.G., Bou Zerdan, R., Seo, D., Cadirov, N., Watanabe, T., Gerbec, J.A., Hawker, C.J., Israelachvili, J.N., Helgeson, M.E.: Triple function lubricant additives based on organic–inorganic hybrid star polymers: friction reduction, wear protection, and viscosity modification. *ACS Appl. Mater. Interfaces* **11**, 1363–1375 (2018)
12. Singh, R.K., Kukrety, A., Kumar, A., Chouhan, A., Saxena, R.C., Ray, S.S., Jain, S.L.: Synthesis, characterization, and performance evaluation of N, N-Dimethylacrylamide–alkyl acrylate copolymers as novel multifunctional additives for lube oil. *Adv. Polym. Technol.* **37**, 1695–1702 (2018)
13. Upadhyay, M., Karmakar, G., Kapur, G.S., Ghosh, P.: Multifunctional greener additives for lubricating oil. *Polym. Eng. Sci.* **58**, 810–815 (2018)
14. Biresaw, G., Bantchev, G.B., Harry-O’Kuru, R.E.: Biobased polyphosphonate additives from methyl linoleates. *Tribol. Trans.* **62**, 428–442 (2019)
15. Yamada, S., Fujihara, A., Yusa, S.I., Tanabe, T., Kurihara, K.: Confined film structure and friction properties of triblock copolymer additives in oil-based lubrication. *Polym. J.* **51**, 41–49 (2019)
16. Robinson, J.W., Zhou, Y., Qu, J., Bays, J.T., Cosimbescu, L.: Highly branched polyethylenes as lubricant viscosity and friction modifiers. *React. Funct. Polym.* **109**, 52–55 (2016)
17. Cosimbescu, L., Robinson, J.W., Zhou, Y., Qu, J.: Dual functional star polymers for lubricants. *RSC Adv.* **6**, 86259–86268 (2016)
18. Marx, N., Ponjavic, A., Taylor, R.I., Spikes, H.A.: Study of permanent shear thinning of VM polymer solutions. *Tribol. Lett.* **65**, 106 (2017)
19. Jeong, S.H., Kim, J.M., Baig, C.: Rheological influence of short-chain branching for polymeric materials under shear with variable branch density and branching architecture. *Macromolecules* **50**, 4491–4500 (2017)
20. Kim, C.A., Kim, J.T., Lee, K., Choi, H.J., Jhon, M.S.: Mechanical degradation of dilute polymer solutions under turbulent flow. *Polymer* **41**, 7611–7615 (2000)
21. Cosimbescu, L., Robinson, J.W., Page, J.P.: Polymer architecture: does it influence shear stability? *Ind. Eng. Chem. Res.* **57**, 11858–11867 (2018)
22. Cosimbescu, L., Vellore, A., Ramasamy, U.S., Burgess, S.A., Martini, A.: Low molecular weight polymethacrylates as multifunctional lubricant additives. *Eur. Polym. J.* **104**, 39–44 (2018)
23. Campbell, K., Erck, R., Swita, M., Cosimbescu, L.: Multifunctional tunable polymethacrylates for enhanced shear stability and wear prevention. *ACS Appl. Polym. Mater.* **2**, 2839–2848 (2020)
24. Qu, J., Chi, M., Meyer, H.M., Blau, P.J., Dai, S., Luo, H.: Nanostructure and composition of tribo-boundary films formed in ionic liquid lubrication. *Tribol. Lett.* **43**, 205–211 (2011)
25. Qu, J., Luo, H., Chi, M., Ma, C., Blau, P.J., Dai, S., Viola, M.B.: Comparison of an oil-miscible ionic liquid and ZDDP as a lubricant anti-wear additive. *Tribol. Int.* **71**, 88–97 (2014)
26. Kohlhauser, B., Ripoll, M.R., Riedl, H., Koller, C.M., Koutna, N., Amsüss, A., Hutter, H., Ramirez, G., Gachot, C., Erdemir, A., Mayrhofer, P.H.: How to get no Wear? A new take on the design of in-situ formed high performing low-friction tribofilms. *Mater. Des.* **190**, 108519 (2020)
27. Kumara, C., Meyer, H.M., III., Qu, J.: Synergistic interactions between silver and palladium nanoparticles in lubrication. *ACS Appl. Nano Mater.* **2**, 5302–5309 (2019)
28. Matsui, Y., Aoki, S., Kurosawa, O., Masuko, M.: Concert and blocking effects of polar compounds on the friction reduction and tribofilm formation of zinc dialkyldithiophosphate. *Tribol. Online* **11**, 417–425 (2016)
29. Pereira, G., Lachenwitzer, A., Munoz-Paniagua, D., Kasrai, M., Norton, P.R., Abrecht, M., Gilbert, P.U.: The role of the cation in antiwear films formed from ZDDP on 52100 steel. *Tribol. Lett.* **23**, 109–119 (2006)
30. Cosimbescu, L., Demas, N.G., Robinson, J.W., Erck, R.A.: Friction-and wear-reducing properties of multifunctional small molecules. *ACS Appl. Mater. Interfaces* **10**, 1317–1323 (2018)
31. Rigney, D.A., Karthikeyan, S.: The evolution of tribomaterial during sliding: a brief introduction. *Tribol. Lett.* **39**, 3–7 (2010)

Publisher’s Note Springer Nature remains neutral with regard to jurisdictional claims in published maps and institutional affiliations.

Authors and Affiliations

Robert A. Erck¹ · Miao Song² · Dongsheng Li² · Lelia Cosimbescu² 

✉ Lelia Cosimbescu
lelia.cosimbescu@pnnl.gov

² Pacific Northwest National Laboratory, Richland, WA 99352, USA

¹ Argonne National Laboratory, Lemont, IL 60439, USA